中国光学 (中英文) Chinese Optics Ei 核心期刊

**带宽可调谐的太赫兹超构材料半波片器件**

吕婷婷 付天舒 刘东明 史金辉

**Bandwidth-tunable terahertz metamaterial half-wave plate component**

LV Ting-ting, FU Tian-shu, LIU Dong-ming, SHI Jin-hui

引用本文:
吕婷婷, 付天舒, 刘东明, 史金辉. 带宽可调谐的太赫兹超构材料半波片器件[J]. 中国光学, 2023, 16(3): 701–714. doi: 10.37188/CO.2022–0198
LV Ting-ting, FU Tian-shu, LIU Dong-ming, SHI Jin-hui. Bandwidth-tunable terahertz metamaterial half-wave plate component[J]. *Chinese Optics*, 2023, 16(3): 701-714. doi: 10.37188/CO.2022-0198

在线阅读 View online: https://doi.org/10.37188/CO.2022–0198

---

文章编号 2097-1842(2023)03-0701-14

# Bandwidth-tunable terahertz metamaterial half-wave plate component

LV Ting-ting[1*], FU Tian-shu[1], LIU Dong-ming[1], SHI Jin-hui[2*]
(1. *School of Physics and Electronic Engineering*, *Northeast Petroleum University*, *Daqing* 163318, *China*;
2. *Key Laboratory of In-Fiber Integrated Optics of Ministry of Education*, *College of Physics and Optoelectronic Engineering*, *Harbin Engineering University*, *Harbin* 150001, *China*)
* *Corresponding author*, *E-mail*: *oktingting521@126.com*; *shijinhui@hrbeu.edu.cn*

**Abstract**: We propose a "leaf-type" hybrid metamaterial to realize bandwidth-tunable half-wave plate based on vanadium dioxide ($VO_2$) phase transition. The hybrid metamaterial is regarded as a hollow "leaf-type" metallic structure and act as a dual-band half-wave plate when $VO_2$ film is in the insulating phase. Within 1.01−1.17 THz and 1.47−1.95 THz, it can accomplish *y*- to *x*-polarization conversion with a polarization conversion rate over 0.9 and an average relative bandwidth of 26%. The metamaterial becomes a solid core "leaf-type" metallic structure when $VO_2$ is in the metallic phase. Within 1.13−2.80 THz, it can act as a broadband half-wave plate with a relative bandwidth of 85%. The working principle of the bandwidth-tunable half-wave plate is explained by the instantaneous surface current distribution and electric field theory in detail. The proposed "leaf-type" hybrid metamaterial half-wave plate has potential application prospects in THz imaging, sensing and polarization detection.

**Key words**: metamaterial; half-wave plate; bandwidth-tunable; terahertz; $VO_2$

# 带宽可调谐的太赫兹超构材料半波片器件

吕婷婷[1*], 付天舒[1], 刘东明[1], 史金辉[2*]
（1. 东北石油大学 物理与电子工程学院, 黑龙江 大庆 163318;
2. 哈尔滨工程大学 物理与光电工程学院, 纤维集成光学教育部重点实验室, 黑龙江 哈尔滨 150001）

**摘要:** 基于二氧化钒(vanadium dioxide, $VO_2$)的相变原理, 提出了一种"树叶型"复合超构材料, 能够实现带宽可调谐的半波片功能。$VO_2$ 薄膜为绝缘态时, 复合超构材料可以看作是空芯"树叶型"金属结构, 能够实现双频带的半波片功能。在 1.01~1.17 THz 和 1.47~1.95 THz 频带范围内能够将 *y* 偏振光转换成 *x* 偏振光, 偏振转换率大于 0.9 且平均相对带宽为 26%。$VO_2$ 薄膜为金属态时, 实芯"树叶型"金属结构的超构材料在 1.13~2.80 THz 范围内能够实现反射型的宽频带半波片功能, 相对带宽为 85%。利用瞬时表面电流分布和电场理论详细地分析了带宽可调谐半波片器件的工作原理。本文所提出的"树叶型"复合超构材料半波片器件在太赫兹成像、传感和偏振探测等领域具有潜在的应用前景。

**关 键 词:** 超构材料; 半波片; 带宽可调谐; 太赫兹; $VO_2$
**中图分类号:** TP394.1; TH691.9 **文献标志码:** A **doi:** 10.37188/CO.2022-0198

**收稿日期:** 2022-09-24; **修订日期:** 2022-11-02
**基金项目:** 国家自然科学基金资助项目(No. U1931121)
Supported by National Natural Science Foundation of China (No. U1931121)

## 1 Introduction

Terahertz (THz) waves usually refers to electromagnetic waves with frequencies in the range of 0.1 to 10 THz[1], which are the transition region between electronics and photonics and occupy an important position in the electromagnetic spectrum. With the rapid development of THz science and technology, high-performance THz devices (e.g., filters, wave plate, beam splitters, and polarization apparatus) are of great research value as key components in THz application systems. In particular, THz polarization converter can effectively control the polarization state of THz waves and has promising applications in polarization spectrum analysis, polarization imaging and THz communication[2-4]. The conventional methods for manipulating the polarization state mainly use the birefringence effect in uniaxial natural crystals to achieve the modulation of the optical field by controlling the phase delay of the two orthogonal polarization components. However, these devices often exhibit narrow operating bands, large losses, large volume and expensive price, which seriously hinder their integrated development and large-scale applications in THz photonic systems.

The emergence of metamaterials has provided a completely new idea to effectively control the polarization state of terahertz waves[5-9]. Metamaterials are artificially designed periodic subwavelength structures whose physical properties depend mainly on its structural design and can achieve extraordinary physical properties that natural materials do not possess[10-14], such as stealth, inverse Doppler effect, and meta-lenses. Currently, terahertz polarization converter based on metamaterials have received extensive attention. Grady N K *et al*. achieved reflective polarization conversion function in the terahertz band using a simple metal cut-wire structure[15]. The cross-polarized reflection is higher than 80% between 0.8 and 1.36 THz, and the co-polarized reflection is lower than 5%. Cheng Y Z *et al*. proposed a reflective half-wave plate device based on multiple resonant responses with a polarization conversion rate higher than 0.8 in the range of 0.65 to 1.45 THz and a relative bandwidth of 76%[16]. Cong L Q *et al*. proposed a metamaterial design consisting of a three-layer inhomogeneous wire grid structure, which can achieve a good polarization rotation function[17]. The efficiency is higher than 80% in the range of 0.6−1.2 THz, and the higher conversion efficiency mainly originates from the Fabry-Perot interference effect in the multilayer structure. On the other hand, the dynamically tunable polarization converter is also a hot research topic. The exquisite design of metamaterials combined with active materials (including graphene[18-19], silicon[20-21], Dirac semimetals[22], and phase change materials[23-25]) provides richness and diversity for polarization tuning. $VO_2$ (Vanadium dioxide), as a typical reversible phase change material, has unique advantages in the design of tunable terahertz devices. It has a phase transition temperature of 68 °C and the conductivity change is 4−5 orders of magnitude during the phase transition under three external excitations: optical, electrical, and thermal, and modulation speeds under optical excitation can reach the sub-picosecond.

Zheng X X *et al*. used the phase transition principle of $VO_2$ to propose a temperature-controlled broadband reflective polarization converter, which can realize the switching functions in the range of 4.95−9.39 THz[26]. Shu F ZH *et al*. combined $VO_2$ and dispersion-free metamaterial to demonstrate experimentally the electrical tuning of broadband polarization effect for the first time[23]. During the phase transition of $VO_2$, the metamaterial was transformed from reflective wave plate to reflective lens. Ding F *et al*. proposed a multilayer hybrid metamaterial design based on the phase transition principle of $VO_2$, which was able to realize the flexible switching of broadband half-wave plate and broadband absorber devices[27], and the bandwidth of half-wave plate was 0.49 THz with reflectivity greater than 60% and polarization conversion rate higher than 95%. Luo J *et al.* used metal-$VO_2$ hybrid metamaterial design to achieve switchable broadband quarter-wave plate and broadband half-wave plate[28]. Yang Z H *et al.* proposed a reflective single-band & broadband half-wave plate device with a relative bandwidth shift from 1.9% to 27% using the voltage-modulated $VO_2$ properties[29]. Most of the reported tunable polarization components are mostly focused on the switching function of a single polarization effect or the conversion function between different polarization effects. However, a relatively little research work has been done on bandwidth-tunable polarization modulation devices, and some of the polarization components have limited bandwidth tuning capability. Bandwidth-tunable wave plate devices have important applications in the fields of polarization detection, polarization imaging and terahertz communication, and deserve more attention.

In this paper, a bandwidth-tunable "leaf-type" hybrid metamaterial is proposed based on the phase transition principle of $VO_2$, which can realize a flexible switching from dual-band to broadband half-wave plate. When $VO_2$ is in the insulating state, the average relative bandwidth of dual-band half-wave plate with PCR greater than 0.90 is 26%. When $VO_2$ is in the metallic state, the relative bandwidth of broadband half-wave plate with PCR greater than 0.90 is 85%. The physical mechanism of the dual-band and broadband polarization conversions is elucidated using the surface current distribution at the resonance. The modulation law of the polarization properties by the oblique incidence angle and the polarization angle is investigated in detail.

## 2 Structural design and numerical simulation

The design of the bandwidth-tunable half-wave plate is derived from the typical sandwich structure, which consists of a hybrid micro-nano structure layer, a polyimide dielectric layer and a continuous metallic aluminum mirror coating (Fig. 1 color online). The hybrid micro-nano structure layer consists of a hollow "leaf-type" metal structure and a solid "leaf-type" $VO_2$ structure. The hybrid metamaterial demonstrates bandwidth-tunable reflective half-wave plate and implements a switchable effect between dual-band and broadband cross-polarization conversion of linearly polarized light during the phase transition of $VO_2$. The solid "leaf-type" $VO_2$ structure is composed of the intersection of two cylindrical structures with mirror symmetry about the plane $x = -y$. Assuming that the coordinates of the center point O of the unit cell structure in the plane $z = 0$ are ($x = 0$ μm, $y = 0$ μm), the coordinates of the corresponding cross-sectional circle centers of the two cylindrical structures in this plane are ($x_1$ = −80 μm, $y_1$ = −50 μm) and ($x_2$ = 80 μm, $y_2$ = 50 μm), respectively. The radius and thickness of the cylindrical $VO_2$ structure are $r$ = 75 μm and $t_m$ = 200 nm, respectively. Similarly, the hollow "leaf-type" metallic structure is obtained from a cylindrical shape with radius $R$ = 80 μm and thickness $t_m$ = 200 nm by a similar process. The thickness of the polyimide is $t$ = 20 μm, side length of unit cell is $a$ = 65 μm and the thickness of the metal mirror layer is $t_m$ = 200 nm. The polarization properties of the hybrid metamaterial are solved using CST full-wave simulation software, with the directions $x$ and $y$ set as the unit cell boundary conditions and the direction $z$ set as the perfectly matched layer boundary condition. The conductivity of metallic aluminum is $3.62 \times 10^7$ S/m, and the dielectric constant of polyimide is 3 and the loss tangent is 0.03[30]. The Drude model is used to describe the material properties of $VO_2$ films at terahertz frequencies as

$$\varepsilon(\omega) = \varepsilon_\infty - \frac{\omega_p^2}{\omega^2 + i\gamma\omega} \quad , \tag{1}$$

where $\varepsilon_\infty$ = 12 is the dielectric constant at infinity frequency and $\gamma = 5.75\times10^{13}$ rad/s is the collision frequency. The plasma frequency $\omega_p$ can be expressed as

$$\omega_p^2 = \omega_p^2(\sigma_0)\frac{\sigma_{VO_2}}{\sigma_0} \quad , \qquad (2)$$

where $\sigma_0 = 3\times10^5$ S/m and $\omega_p(\sigma_0) = 1.4\times10^{15}$ rad/s. $\sigma_{VO_2}$ is the conductivity of $VO_2$, and the phase states of $VO_2$ at different temperatures can be characterized by conductivity values of 10 S/m and $2\times10^5$ S/m for the insulating and metallic states, respectively[31]. The reflection coefficient is denoted as $R_{ij}$ ($r_{ij} = |R_{ij}|$), and the subscripts $i$ and $j$ represent the polarization states of the reflected and incident light, respectively. In order to ensure the temperature uniformity of the "leaf-type" metamaterial, a temperature-controlled heating plate with holes is introduced for the actual polarization performance measurement, considering the temperature-controlled phase transition of $VO_2$. The temperature control is achieved by means of Pt resistors and temperature sensors inside the heating plate and a temperature control unit connected to them[32]. Moreover, it is important to emphasize that the temperature regulation of $VO_2$ generally operates at temperatures between 25 °C and 88 °C[31, 33], and this operating temperature range does not affect the material properties of the dielectric layer polyimide and the metal structure.

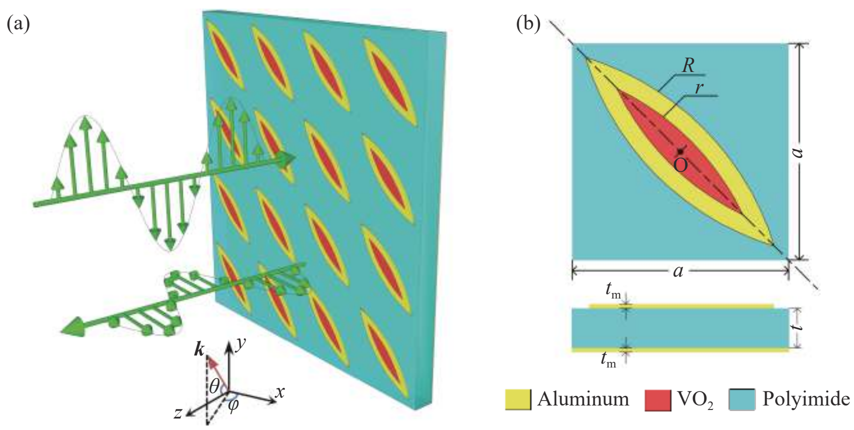


Fig. 1 Operation principle of “leaf-type” hybrid metamaterial and it’s structural diagram. (a) Schematic diagram of half-wave plate (The polarization angle $\varphi$ and incident angle $\theta$ are marked in the inset); (b) structural parameters of a unit cell in the proposed metamaterial

图 1 “树叶型”复合超构材料的工作原理和结构示意图。(a)半波片工作原理图(偏振旋转角 $\varphi$ 和倾斜入射角 $\theta$ 已在插图中标注);(b)基本单元的结构参数图

At room temperature, the $VO_2$ film is in the insulating state, and the hybrid metamaterial can be seen as a hollow core "leaf-type" metallic structure. In the ranges of 1.08−1.83 THz and 2.48−2.63 THz, the reflection coefficient $r_{xy}$ is greater than 0.8 and the maximum value is 0.92, while $r_{yy}$ is less than 0.44, as shown in Fig. 2(a). To further evaluate the polarization conversion ability of the metamaterial, the Polarization Conversion Rate (PCR) is used to describe as

$$\mathrm{PCR} = \frac{|R_{xy}|^2}{|R_{xy}|^2 + |R_{yy}|^2} \quad . \qquad (3)$$

The higher PCR indicates that the ability of cross-polarization conversion is more powerful. The PCR of the hybrid metamaterial stays above 0.9 in the ranges of 1.01−1.17 THz and 1.47−1.95 THz, and even approaches 1 at 1.22 THz and 1.68 THz, as shown in Fig. 2(c), indicating that the incident $y$-polarized light can be efficiently converted to $x$-polarized light in the range of dual frequency bands. Further, to clarify the advantages and disadvantages of the operating bandwidth of the device, the relative bandwidth of the component is defined as the ratio of the bandwidth width ($\Delta f$) to the center frequency $f_0$, i.e., $\Delta f/f_0$. The average relative bandwidth

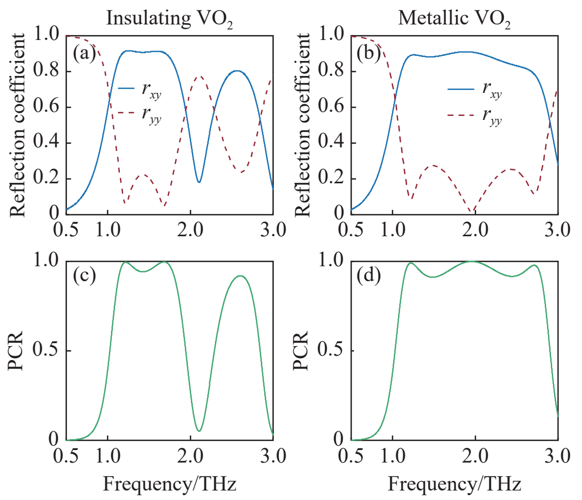


Fig. 2　Reflection polarization properties of “leaf-type” hybrid metamaterial when the $VO_2$ film is in different phase states. (a) and (b) Reflection coefficients of co- and cross-polarization; (c) and (d) Polarization Conversion Ratio (PCR)

图 2　$VO_2$ 薄膜为不同相态时“树叶型”复合超构材料的反射偏振特性。(a)和(b)共偏振和正交偏振反射系数;(c)和(d)偏振转换率

of the hollow "leaf-type" metamaterial at room temperature with a PCR greater than 0.90 is 26%. When the temperature reaches above the phase transition temperature of the $VO_2$ film, the $VO_2$ film has metal-like properties and the hybrid metamaterial is transformed into a solid "leaf-type" metallic structure. Within the frequency range from 1.10 to 2.69 THz, the reflection coefficient $r_{xy}$ is greater than 0.8 and the maximum value is 0.91, while $r_{yy}$ is less than 0.37, as shown in Fig. 2(b). The PCR is higher than 0.9 in the range of 1.13−2.80 THz, and approaches to 1 at 1.95 THz and 2.71 THz, as shown in Fig. 2(d). The relative bandwidth is 85% with PCR above 0.90 for the solid "leaf-type" metamaterial.

The polarization ellipse of the hybrid metamaterial at the PCR resonant frequency is given in Fig. 3. when $VO_2$ is in the insulating state, the polarization state of the reflected electric field is approximately $x$-polarized light at 1.22 THz and 1.68 THz, indicating that the metamaterial is able to convert the incident $y$-polarized light almost completely into its cross-polarization state, and its function can be analogous to that of a half-wave plate device. To clarify the polarization information of the output reflected light, the polarization elliptical azimuth angle $\psi$ and ellipticity angle $\eta$ can be used to quantify:

$$\tan(2\psi) = \frac{2r}{1-r^2}\cos(\Delta\varphi) \quad , \qquad (4)$$

$$\sin(2\eta) = \frac{2r}{1+r^2}\sin(\Delta\varphi) \quad , \qquad (5)$$

where $r = r_{yy}/r_{xy}$ represents the amplitude ratio between the two orthogonal components, and $\triangle\varphi = \varphi_{yy} - \varphi_{xy}$ represents the phase difference between them. The polarization elliptical azimuth (ellipticity) angles of reflected $x$-polarized light at 1.22 THz and 1.68 THz are 3.7° (−0.04°) and −2.9° (1.3°), respectively, and the polarization elliptical azimuth angle and ellipticity angle at 2.61 THz are −0.5° and 16.8°, respectively. The above results quantitatively explain the cross-polarization conversion of the metamaterial. The polarization elliptical azimuth (ellipticity) angles at the three PCR resonant frequencies are 5.4° (0.6°), −1° (−0.3°), and 7.7° (−4.18°) with metallic $VO_2$ at high temperature, respectively. These results further indicate that the solid metal "leaf-type" hybrid metamaterial has the functional properties of a half-wave plate.

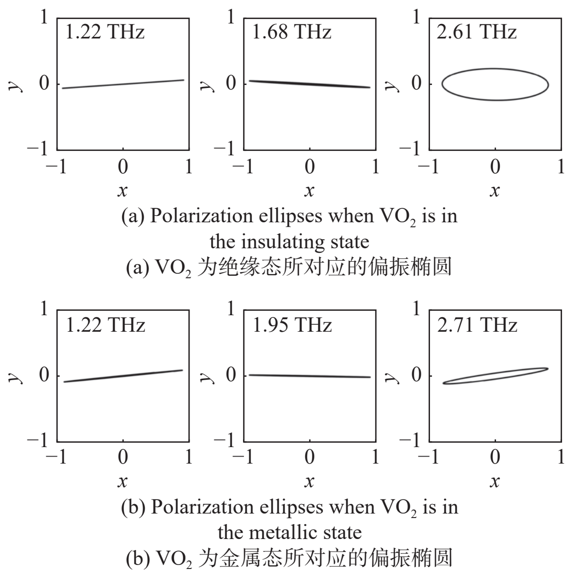


Fig. 3　Polarization ellipses of reflected lights at the six specific frequencies under $y$-polarized illumination.

图 3　$y$ 偏振光激发下 6 个特定频率处的偏振椭圆

## 3 Analysis of the working principle of the half-wave plate

In order to explore the working principle of the half-wave plate in detail, the normally incident $y$-polarized light is decomposed into two electric field components along the axes $u$ and $v$, and the incident and reflected electric fields are

$$\boldsymbol{E}_{\rm i} = \hat{\boldsymbol{u}} E_{{\rm i}u} + \hat{\boldsymbol{v}} E_{{\rm i}v} \quad . \tag{6}$$

$$\boldsymbol{E}_{\rm r} = \left(\hat{\boldsymbol{u}} r_{uu} e^{{\rm i}\varphi_{uu}} + \hat{\boldsymbol{v}} r_{vu} e^{{\rm i}\varphi_{vu}}\right) E_{{\rm i}u} + \left(\hat{\boldsymbol{v}} r_{vv} e^{{\rm i}\varphi_{vv}} + \hat{\boldsymbol{u}} r_{uv} e^{{\rm i}\varphi_{uv}}\right) E_{{\rm i}v} . \tag{7}$$

Since the structure of the "leaf-type" metamaterial is perfectly symmetric about the axes $u$ and $v$, the cross-polarization conversion reflection coefficients $r_{uv}$ and $r_{vu}$ are zero, and the polarization state of the reflected light depends mainly on the co-polarization reflection coefficients and phase information. At room temperature, within the frequency range of 1.13~1.81 THz and 2.52~2.67 THz, the amplitudes of the two co-polarization coefficients are almost equal ($r_{uu} \approx r_{vv}$) and the phase difference ($\Delta\varphi = \varphi_{uu} - \varphi_{vv}$) shows ±180° (±30°), as shown in Figs. 4(a) and 4(c) (color online). Therefore, when the $VO_2$ film is in the insulating state, the "leaf-type" hybrid metamaterial can be regarded as a dual-band half-wave plate device. Fig.s 4(b) and 4(d) (color online) show that the co-polarization transmission coefficient and phase difference also satisfy the two key conditions for realizing the half-wave plate in the range of 1.13−2.80 THz at high temperature. Therefore, the hybrid metamaterial is capable of realizing the broadband half-wave plate when the $VO_2$ film is in the metallic state.

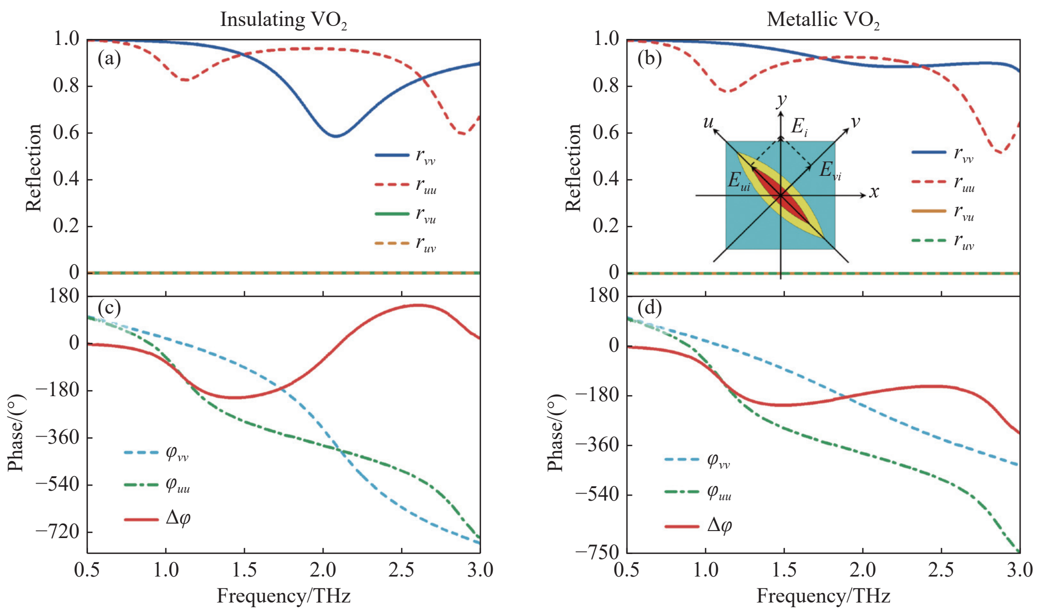


Fig. 4 Reflection coefficients and phases of the hybrid metamaterial for normal $u$ and $v$ polarization incidences when the $VO_2$ film is in different phase states. (a) and (b) Reflection coefficients $r_{uu}$, $r_{vv}$ and $r_{uv}$, $r_{vu}$; (c) and (d) reflection phases $\varphi_{uu}$, $\varphi_{vv}$ and phase difference $\Delta\varphi$ (normal $u$ and $v$ polarization incidences, as depicted by the inset)

图 4 $VO_2$ 薄膜为不同相态时，垂直入射的 $u$ 偏振和 $v$ 偏振激发“树叶型”复合超构材料的反射系数和相位频谱图。(a)和(b)反射系数 $r_{uu}$, $r_{vv}$ 和 $r_{uv}$, $r_{vu}$；(c)和(d)$\varphi_{uu}$ 和 $\varphi_{vv}$ 及其相位差 $\Delta\varphi$($u$ 偏振和 $v$ 偏振如插图所示)

In order to investigate the physical mechanism of the polarization conversion effect of the "bandwidth-tunable" half-wave plate device, the instantaneous surface current distribution of the "leaf-type" hybrid metamaterial at the PCR resonant frequency is shown in Fig. 5 (color online). When $VO_2$ is in the insulating state, the surface currents at resonant frequencies of 1.22 THz, 1.68 THz, 2.10 THz and 2.61 THz are shown in Fig. 5(a) to (d). At 1.22 THz, the surface currents are mainly concentrated in the inner and outer sides of the hollow "leaf-type" structure, and the current direction is opposite to the current of the underlying mirror coating, which excites the magnetic dipole response, as shown in Fig. 5(a). At 1.68 THz and 2.61 THz, the surface currents are mainly distributed at the inner ends of the hollow "leaf-type" structure, and the current direction of the top "leaf-type" structure is opposite to that of the underlying mirror coating at 1.68 THz, resulting in a magnetic dipole response. At 2.61 THz, the surface currents are in the same direction to that of the underlying mirror coating and the electric dipole response is excited, as shown in Fig. 5(b) and 5(d). For the resonant valley position at 2.10 THz, the surface currents are distributed at the inner end of the hollow "leaf-type" structure, as shown in Fig. 5(c). However, the current of the top and bottom structures will not produce significant dipole response, so the cross-polarization conversion effect at this resonant frequency is weak. For $VO_2$ in the metallic state, the magnetic dipole response is excited at 1.22 THz, which is the same response mechanism as that in the insulating state at this frequency. The only difference is that $VO_2$ in the metallic state causes the surface currents to be distributed mainly on the outer side of the solid "leaf-type" structure, as shown in Fig. 5(e). At the resonant frequencies of 1.95 THz and 2.71 THz, the efficient cross-polarization conversion effects are derived from magnetic dipole and electric dipole response, respectively, as shown in Fig. 5(f) and 5(h). In particular, it can be seen from Fig. 5(g) that the solid "leaf-type" hybrid metamaterial also excites a significant electric dipole response at 2.10 THz, which is completely different from the resonant response at this frequency in the insulating state. Therefore, the bandwidth-tunable half-wave plate device is mainly realized by the superposition of multiple electric and magnetic dipole resonant responses.

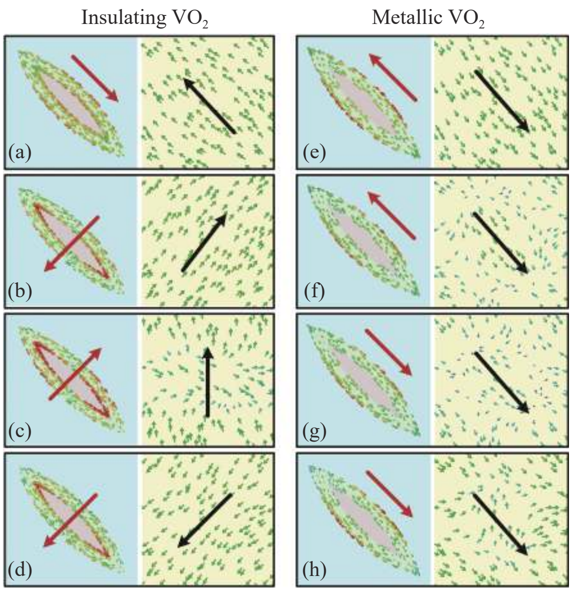


Fig. 5　Instantaneous surface current distributions at critical frequencies. (a) 1.22 THz, (b) 1.68 THz, (c) 2.10 THz, (d) 2.61 THz for $VO_2$ film in the complete insulating state; (e) 1.22 THz, (f) 1.95 THz, (g) 2.10 THz, (h) 2.71 THz for $VO_2$ film in the complete metallic state

图 5　关键频率处的瞬时表面电流分布图。$VO_2$ 为绝缘态时，(a) 1.22 THz、(b) 1.68 THz、(c) 2.10 THz、(d) 2.61 THz; $VO_2$ 为金属态时，(e) 1.22 THz、(f) 1.95 THz、(g) 2.10 THz、(h) 2.71 THz

## 4　Angle modulation law of half-wave plate characteristics

The relationship between the half-wave plate properties of the "leaf-type" hybrid metamaterial and the incident angle and polarization angle is shown in Figs. 6 and 7 (color online). When the $VO_2$ film is in the insulating state, the half-wave plate characteristics with the cross-reflection coefficient $r_{xy}$ greater than 0.8 are applicable from 0° to 46° in the range of 1.22 to 1.68 THz. In particular, the $r_{xy}$ is greater than 0.8 and the PCR is greater than 90% at the center of 1.22 THz in the incident angle range of 0°−70°, as shown in Fig. 6(a) and 6(c). The properties of the half-wave plate at high frequencies have good polarization conversion in the range of 0°−30°. When the $VO_2$ film is in the metallic state,

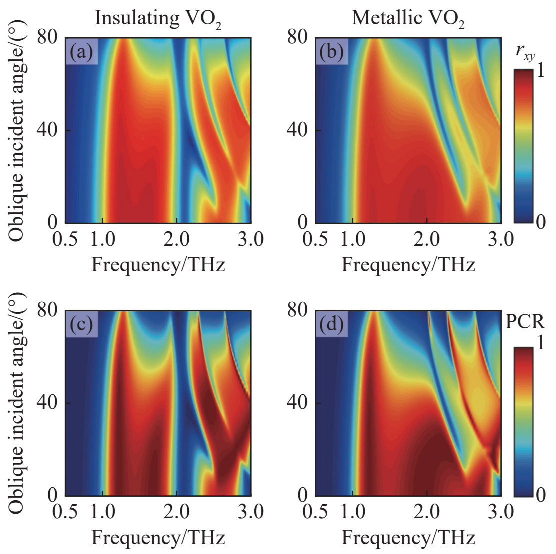


Fig. 6 Incident angle dependence of bandwidth-tunable half-wave plate components when $VO_2$ film is in the complete insulating and metallic states. (a) and (b) $r_{xy}$; (c) and (d) PCR

图 6 $VO_2$ 薄膜为绝缘态和金属态时，带宽可调谐半波片器件随入射角度 $\theta$ 的变化规律。(a)和(b)$r_{xy}$；(c)和(d)PCR

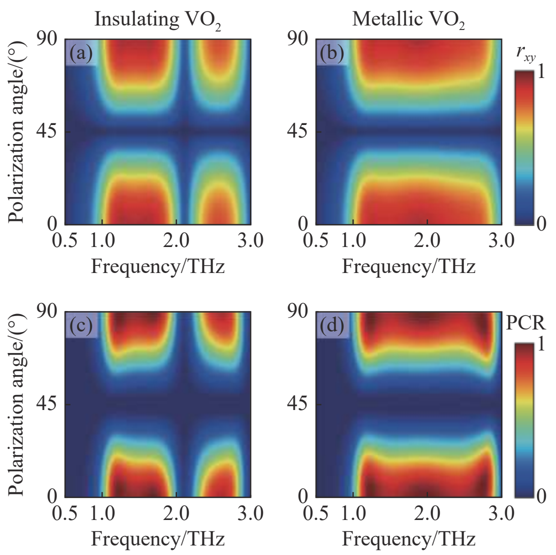


Fig. 7 Polarization angle dependence of bandwidth-tunable half-wave plate components when $VO_2$ film is in the complete insulating and metallic states. (a) and (b) $r_{xy}$; (c) and (d) PCR

图 7 $VO_2$ 薄膜为绝缘态和金属态时带宽可调谐半波片器件随偏振角度的变化规律。(a)和(b)$r_{xy}$；(c)和(d)PCR

the broadband half-wave plate do not have good working performance at oblique incidence angles, as shown in Fig. 6(b) and 6(d). However, the properties in the range of 1.20 to 2.20 THz are similar to the angle-dependent properties at low frequencies of the insulating state. Regardless of whether the $VO_2$ film is in the insulating or metallic state, it has significant multiband angular dispersion properties at high frequencies, which originate from the near-field coupling effect between the unit cells[34]. Fig. 7 shows that the bandwidth-tunable half-wave plate devices exhibit a significant angular dependence of polarization. Interestingly, the half-wave plate properties between 0°−45° and 45°−90° polarization angles satisfy symmetry with respect to 45° polarization, while the cross-polarization conversion effect completely disappears as the polarization angle approaches 45°. This is closely related to the two-fold rotational symmetry of the "leaf-type" structure with respect to the −45° polarization direction.

## 5 Conclusion

In this paper, a "leaf-type" hybrid metamaterial design is proposed to realize the function of reflective half-wave plate with tunable bandwidth through the temperature-controlled phase transition of $VO_2$, and the hybrid metamaterial can realize the switching of dual-band and broadband half-wave plate during the phase transition, and the relative bandwidth is changed from 26% to 85% with the PCR greater than 0.9. The physical mechanism of the bandwidth-tunable half-wave plate is explained using the surface current distribution at the resonant frequency, and the effective superposition of multiple electric and magnetic dipole resonance responses achieves the bandwidth-tunable half-wave plate function. The modulation law at oblique incident angle and polarization angle of half-wave plate is investigated in detail. The proposed bandwidth-tunable terahertz metamaterial facilitates the design of polarization-modulated devices and provides an idea for the development of miniaturized and integrated terahertz systems.

——中文对照版——

# 1　引　言

太赫兹波(THz)通常是指频率在 0.1~10 THz 范围内的电磁波[1], 是电子学和光子学之间的过渡区域, 在电磁波谱中占据着重要位置。随着 THz 科学与技术的快速发展, 高性能 THz 器件(例如: 滤波器、波片、分束器和偏振器件等)作为 THz 应用系统中的关键组成部分, 具有重要的研究价值。特别地, THz 偏振转换器件由于能够有效控制 THz 波的偏振态, 在偏振频谱分析、偏振成像和 THz 通信领域具有广阔的应用前景[2-4]。操控偏振态的传统方法主要是利用单轴自然晶体中的双折射效应, 通过控制两个正交偏振分量的相位延迟实现对光场的调控。然而, 这些器件往往呈现出工作频带窄、损耗大、体积大且价格昂贵的特点, 严重地阻碍了其在 THz 光子系统中的集成化发展和大规模应用。

超构材料(Metamaterials)的出现为有效控制太赫兹的偏振态提供了一个全新思路[5-9]。超构材料是一种人工设计的周期性亚波长结构, 其物理特性主要依赖于它的结构设计, 能够实现自然材料所不具备的超常物理特性[10-14], 例如: 隐身、逆多普勒效应和超构透镜等。目前, 基于超构材料的太赫兹偏振转换器件得到了广泛的关注。Grady N K 等利用简单的金属切割线结构实现了太赫兹频段的反射型偏振转换功能[15]。在 0.8~1.36 THz 之间正交偏振光的反射率高于 80%, 且共偏振反射率低于 5%。Cheng Y Z 等基于多重谐振响应提出一种反射型的半波片器件, 在 0.65~1.45 THz 范围内偏振转换率高于 0.8, 相对带宽为 76%[16]。Cong L Q 等提出一种由三层不均匀线栅结构组成的超构材料设计, 能够实现良好的偏振旋转功能[17], 在 0.6~1.2 THz 范围内透射光效率高于 80%, 较高的转换效率主要源于多层结构中的法布里-泊罗干涉效应。另一方面, 动态可调控的偏振转换器件也是研究的热点。超构材料结合有源材料(包括石墨烯[18-19]、硅[20-21]、狄拉克半金属[22] 和相变材料[23-25] 等)的精巧设计为偏振调控提供了丰富性和多样性。二氧化钒(vanadium dioxide, $VO_2$)作为一种典型的可逆型相变材料, 在可调谐太赫兹器件的设计中具有独特的优势。它的相变温度为 68°C, 在光、电和热 3 种外部激励下, 电导率突变量都能够达到 4~5 个量级, 且光激励下的调制速度能够达到亚皮秒量级。

Zheng X X 等利用 $VO_2$ 的相变原理提出一种温控的宽频带反射型偏振转换器件, 能够实现 4.95~9.39 THz 的开关功能[26]。Shu F ZH 等结合 $VO_2$ 和无色散超构材料首次实验实现了电控的宽频带偏振效应[23]。在 $VO_2$ 相变过程中, 超构材料由反射型波片转变为反射型透镜功能。Ding F 等基于 $VO_2$ 的相变原理提出多层复合超构材料设计, 能够实现宽频带半波片和宽频带吸收器件的灵活转换功能[27], 反射率大于 60% 且偏振转换率高于 95% 的半波片带宽为 0.49 THz。Luo J 等利用金属-$VO_2$ 的复合超构材料设计, 实现了可开关的宽频带四分之一波片和宽频带半波片功能[28]。Yang Z H 等利用电压调控 $VO_2$ 的特性, 提出一种反射型单频带-宽频带的半波片器件, 相对带宽由 1.9% 转变为 27%[29]。

现已报道的大部分可调谐偏振器件多集中于单一偏振效应的开关功能或是不同偏振效应之间的转换功能。然而, 带宽可调谐偏振调控器件的研究工作相对较少, 且部分偏振器件的带宽调谐能力有限。带宽调谐型的波片器件在偏振探测、偏振成像和太赫兹通信等领域具有重要的应用价值, 值得更多的关注。

本文基于 $VO_2$ 的相变原理提出一种带宽可调谐的“树叶型”复合超构材料, 能够实现双频带和宽频带的半波片转换功能。$VO_2$ 为绝缘态时, 双频带半波片 PCR 大于 0.90 的平均相对带宽为 26%。$VO_2$ 为金属态时, 宽频带半波片 PCR 大于 0.90 的相对带宽为 85%。利用谐振处的表面电流分布阐明了双频带和宽频带偏振转换的物理机制。详细地研究了倾斜入射角度和偏振角度对偏振特性的调制规律。

# 2　结构设计和数值仿真

带宽可调谐半波片的超构材料设计借鉴典型

的三明治结构，主要包括复合微纳结构层、聚酰亚胺(polyimide)介质层和连续的金属铝反射镜层(图 1，彩图见期刊电子版)。复合微纳结构层由空芯“树叶型”金属结构和实芯“树叶型”$VO_2$ 结构组成。$VO_2$ 薄膜相变的过程中，复合超构材料呈现出带宽可调谐的反射型半波片功能，实现了反射型的双频带到宽频带的线偏振光正交偏振转换效应。实芯“树叶型”$VO_2$ 结构是由两个关于 $x=-y$ 平面镜像对称的圆柱形结构的交集部分组成。假定基本单元结构在 $z=0$ 平面上的中心点 O 的坐标为($x=0$ μm, $y=0$ μm)，则两个圆柱结构在该平面上所对应的横截面圆心坐标分别为($x_1=-80$ μm, $y_1=-50$ μm)和($x_2=80$ μm, $y_2=50$ μm)。圆柱形 $VO_2$ 结构的半径和厚度分别为 $r=75$ μm 和 $t_m=200$ nm。同理，空芯“树叶型”金属结构是由半径 $R=80$ μm和厚度 $t_m=200$ nm 的圆柱形经过相似处理获得的。聚酰亚氨的厚度 $t=20$ μm，基本单元的边长为 $a=65$ μm，金属反射镜层的厚度 $t_m=200$ nm。利用 CST 全波仿真软件求解复合超构材料的偏振特性，$x$ 和 $y$ 方向设置为基本单元边界条件，$z$ 方向是完美匹配层边界条件。金属铝的电导率为 $3.62\times10^7$ S/m, polyimide 的介电常数为 3 且损耗正切为 0.03[30]。利用 Drude 模型描述太赫兹频率处 $VO_2$ 薄膜的材料特性:

$$\varepsilon(\omega)=\varepsilon_\infty-\frac{\omega_p^2}{\omega^2+i\gamma\omega} \quad , \tag{1}$$

其中 $\varepsilon_\infty=12$ 是无穷大频率处的介电常数，$\gamma=5.75\times10^{13}$ rad/s 为碰撞频率。等离子频率 $\omega_p$ 可表示为:

$$\omega_p^2=\omega_p^2(\sigma_0)\frac{\sigma_{VO_2}}{\sigma_0} \quad , \tag{2}$$

其中 $\sigma_0=3\times10^5$ S/m 和 $\omega_p(\sigma_0)=1.4\times10^{15}$ rad/s。$\sigma_{VO_2}$ 是 $VO_2$ 的电导率，$VO_2$ 在不同温度下的相态可以用电导率值来表征，绝缘态和金属态的电导率值分别为 10 S/m 和 $2\times10^5$ S/m[31]。反射系数表示为 $R_{ij}$ ($r_{ij}=|R_{ij}|$)，下标 $i$ 和 $j$ 分别代表的是反射光和入射光的偏振态。考虑到采用温度调控 $VO_2$ 的相变特性，因此在实际的偏振性能测量中，为了保证“树叶型”超构材料的温度均匀性，需要引入温度可控的带孔加热板。通过加热板内部的 Pt 电阻和温度传感器以及连接它们的温度控制单元实现温度控制[32]。而且，需要强调一点，温度调控 $VO_2$ 时，工作温度一般在 25~88 °C[31,33]，这个工作温度范围不会影响介质层聚酰亚氨和金属结构部分的材料特性。

常温下，$VO_2$ 薄膜为绝缘态，复合超构材料可看作空芯的“树叶型”金属结构。在 1.08~1.83 THz 和 2.48~2.63 THz 频率范围内，反射系数 $r_{xy}$ 大于 0.8 且最大值为 0.92，而 $r_{yy}$ 小于 0.44，如图 2(a)所示。为了进一步评价超构材料的偏振转换能力，利用偏振转换率(Polarization Conversion Rate, PCR)来描述:

$$\mathrm{PCR}=\frac{|R_{xy}|^2}{|R_{xy}|^2+|R_{yy}|^2} \quad . \tag{3}$$

参数 PCR 越高表明超构材料正交偏振转换的能力越强。在 1.01~1.17 THz 和 1.47~1.95 THz 的频率范围内，复合超构材料的 PCR 保持在 0.9 以上，甚至在 1.22 THz 和 1.68 THz 处接近于 1。由图 2(c)可见在双频带范围内入射的 $y$ 偏振光能够高效地转换成 $x$ 偏振光。进一步，为了明确器件的工作带宽优劣，定义器件的相对带宽为带宽宽度($\Delta f$)与中心频率 $f_0$ 之比，即: $\Delta f/f_0$。常温下，空芯“树叶型”超构材料的 PCR 大于 0.90 时的平均相对带宽为 26%。当温度达到 $VO_2$ 薄膜相变温度以上，$VO_2$ 薄膜具有类金属特性，复合超构材料转变为实芯的金属“树叶型”结构。在 1.10~2.69 THz 频率范围内，反射系数 $r_{xy}$ 大于 0.8 且最大值为 0.91，而 $r_{yy}$ 小于 0.37，如图 2(b)所示。PCR 值在 1.13~2.80 THz 范围内均高于 0.9，且在 1.95 THz 和 2.71 THz 接近于 1，如图 2(d)所示。实芯“树叶型”超构材料的 PCR 大于 0.90 的相对带宽为 85%。

图 3 给出了复合超构材料在 PCR 谐振频率处的偏振椭圆。$VO_2$ 为绝缘态时，在 1.22 THz 和 1.68 THz 处，反射电场的偏振态近似为 $x$ 偏振光，表明超构材料能够将入射的 $y$ 偏振光几乎完全转换成它的正交偏振态，其功能可类比于半波片器件。为了明确输出反射光的偏振信息，可以采用偏振椭圆方位角 $\psi$ 和椭圆度角$\eta$来量化:

$$\tan(2\psi)=\frac{2r}{1-r^2}\cos(\Delta\varphi) \quad , \tag{4}$$

$$\sin(2\eta)=\frac{2r}{1+r^2}\sin(\Delta\varphi) \quad , \tag{5}$$

其中 $r = r_{yy}/r_{xy}$ 表示两个正交分量之间的幅度比，$\Delta\varphi = \varphi_{yy} - \varphi_{xy}$ 代表它们之间的相位差。反射 $x$ 偏振光在 1.22 THz 和 1.68 THz 处的偏振椭圆方位(椭圆度)角分别是 3.7°(−0.04°)和−2.9°(1.3°)，2.61 THz 处的偏振椭圆方位角度和椭圆度角分别为−0.5°和 16.8°，以上结果定量地解释了超构材料的正交偏振转换效应。高温时，$VO_2$ 为金属态时，在 3 个 PCR 谐振频率处的偏振椭圆方位(椭圆度)角分别是 5.4°(0.6°)、−1°(−0.3°)和 7.7°(−4.18°)。这些结果进一步表明实芯金属“树叶型”复合超构材料具有半波片功能特性。

## 3 半波片工作原理分析

为了详细探究半波片的工作原理，将垂直入射的 $y$ 偏振光分解为沿 $u$ 轴和 $v$ 轴方向的两个电场分量，则入射和反射电场分别为：

$$\boldsymbol{E}_{\rm i} = \hat{\boldsymbol{u}}E_{{\rm i}u} + \hat{\boldsymbol{v}}E_{{\rm i}v} \quad . \tag{6}$$

$$\boldsymbol{E}_{\rm r} = \left(\hat{\boldsymbol{u}}r_{uu}e^{{\rm i}\varphi_{uu}} + \hat{\boldsymbol{v}}r_{vu}e^{{\rm i}\varphi_{vu}}\right)E_{{\rm i}u} + \left(\hat{\boldsymbol{v}}r_{vv}e^{{\rm i}\varphi_{vv}} + \hat{\boldsymbol{u}}r_{uv}e^{{\rm i}\varphi_{uv}}\right)E_{{\rm i}v} . \tag{7}$$

由于“树叶型”超构材料结构关于 $u$ 轴和 $v$ 轴完全对称，故正交偏振转换反射系数 $r_{uv}$ 和 $r_{vu}$ 为 0，则反射光的偏振态主要取决于共偏振反射系数和相位信息。常温时，在 1.13~1.81 THz 和 2.52~2.67 THz 的频率范围内，两个共偏振系数的幅度几乎相等($r_{uu} \approx r_{vv}$)并且相位差 ($\Delta\varphi = \varphi_{uu} - \varphi_{vv}$) 呈现出±180°(±30°)的特性，如图 4(a)和 4(c)(彩图见期刊电子版)所示。因此，$VO_2$ 薄膜为绝缘态时，“树叶型”复合超构材料可以看作是双频带的半波片器件。图 4(b)和 4(d)(彩图见期刊电子版)表明：高温时，在 1.13~2.80 THz 范围内，共偏振透射系数和相位差同样满足实现半波片的两个关键条件。因此，$VO_2$ 薄膜为金属态时，复合超构材料能够实现宽频带的半波片功能。

为了探究“带宽可调谐”半波片器件偏振转换效应的物理机制，“树叶型”复合超构材料在 PCR 谐振频率处的瞬时表面电流分布如图 5(彩图见期刊电子版)所示。当 $VO_2$ 为绝缘态时，谐振频率分别为 1.22 THz、1.68 THz、2.10 THz 和 2.61 THz 处的表面电流分布如图 5(a)~5(d)所示。在 1.22 THz 处，表面电流主要集中于空芯“树叶型”结构的内外两侧，而且其表面电流与底层金属镜反射层的电流方向相反，激发出磁偶极子响应，如图 5(a)所示。在 1.68 THz 和 2.61 THz 处，表面电流主要分布在空芯“树叶型”结构的内部两端。1.68 THz 频率处，顶层“树叶型”结构与底层金属层的电流方向相反，产生了磁偶极子响应。而 2.61 THz 处表面电流方向相同，激发了电偶极子响应，如图 5(b)和 5(d)所示。对于 2.10 THz 处的谐振谷位置，表面电流分布于空芯“树叶型”结构的内端，如图 5(c)所示。但是顶层与底层结构的电流不会产生显著的偶极子响应，因此，在这个谐振频率处的正交偏振转换效应较弱。$VO_2$ 为金属态时，1.22 THz 处激发出磁偶极子响应，与绝缘态在此频率处的响应机制相同。唯一不同的是，$VO_2$ 的金属态特性使得表面电流主要分布在实芯“树叶型”结构的外侧，如图 5(e)所示。对于 1.95 THz 和 2.71 THz谐振频率处，分别是由磁偶极子和电偶极子响应导致的高效的正交偏振转换效应，如图 5(f)和(h)所示。特别地，由图 5(g)可知，在 2.10 THz 处实芯“树叶型”复合超构材料同样地激发了显著的电偶极子响应，这与绝缘态时此频率处的谐振响应完全不同。因此，带宽可调谐半波片器件主要是由多重电偶极子和磁偶极子谐振响应叠加实现的。

## 4 半波片特性的角度调制规律

“树叶型”复合超构材料的半波片特性与入射角度和偏振角度的关系如图 6 和 7(彩图见期刊电子版)所示。当 $VO_2$ 薄膜为绝缘态时，正交反射系数 $r_{xy}$ 大于 0.8 的半波片特性在 1.22~1.68 THz 内的适用角度为 0~46°。特别地，以 1.22 THz 为中心的工作频带在 0~70°的入射角度范围内 $r_{xy}$ 大于 0.8 且 PCR大于 90%，如图 6(a)和 6(c)所示。而高频处的半波片特性在 0~30°内具有良好的偏振转换特性。当 $VO_2$ 薄膜为金属态时，宽频带的半波片特性在倾斜入射角度下不具有良好的工作性能，如图 6(b)和 6(d)所示。然而，其在 1.20~2.20 THz 范围内的半波片特性与绝缘态低频处的角度依赖特性相似。无论 $VO_2$ 薄膜是处于绝缘态还是金属态，在高频率处都具有显著的多频带角度色散特性，这种角度色散特性源于基本结构单元之间的近场耦合效应[34]。图 7

表明带宽可调谐半波片器件呈现出明显的偏振角度依赖性。有趣的是，在 0~45°和 45°~90°偏振角之间的半波片特性相对于 45°偏振满足对称特性，而当偏振角接近 45°时，正交偏振转换效应完全消失。这与“树叶型”结构关于−45°偏振方向具有二重旋转对称性紧密相关。

## 5 结　论

本文提出一种“树叶型”复合超构材料设计方法，通过温度调控 $VO_2$ 的相变特性实现了带宽可调谐的反射型半波片功能。在 $VO_2$ 相变过程中，复合超构材料能够实现双频带-宽频带的半波片功能，其 PCR 大于 0.9 的相对带宽由 26% 转变为 85%。利用谐振频率处的表面电流分布解释了带宽可调谐半波片器件的物理机制，多重电偶极子和磁偶极子谐振响应的有效叠加实现了带宽可调谐的半波片功能。详细地研究了倾斜入射角度和偏振角度对半波片特性的调制规律。本章所提出的带宽可调谐太赫兹超构材料有利于偏振调控器件的设计并为发展小型化和集成化太赫兹系统提供了一种思路。

**References:**


[1] KLEINER R. Filling the terahertz gap[J]. *Science*, 2007, 318(5854): 1254-1255.

[2] LI J T, LI J, ZHENG C L, *et al*.. Active controllable spin-selective terahertz asymmetric transmission based on all-silicon metasurfaces[J]. *Applied Physics Letters*, 2021, 118(22): 221110.

[3] LIU SH, CUI T J, XU Q, *et al*.. Anisotropic coding metamaterials and their powerful manipulation of differently polarized terahertz waves[J]. *Light:Science & Applications*, 2016, 5(5): e16076.

[4] LI J, ZHENG CH L, WANG G C, *et al*.. Circular dichroism-like response of terahertz wave caused by phase manipulation via all-silicon metasurface[J]. *Photonics Research*, 2021, 9(4): 567-573.

[5] WU SH, ZHANG ZH, ZHANG Y, *et al*.. Enhanced rotation of the polarization of a light beam transmitted through a silver film with an array of perforated *S*-shaped holes[J]. *Physical Review Letters*, 2013, 110(20): 207401.

[6] HAO J M, YUAN Y, RAN L X, *et al*.. Manipulating electromagnetic wave polarizations by anisotropic metamaterials[J]. *Physical Review Letters*, 2007, 99(6): 063908.

[7] ZHELUDEV N I, PLUM E, FEDOTOV V A. Metamaterial polarization spectral filter: isolated transmission line at any prescribed wavelength[J]. *Applied Physics Letters*, 2011, 99(17): 171915.

[8] MA W, CHENG F, LIU Y M. Deep-learning-enabled on-demand design of chiral metamaterials[J]. *ACS Nano*, 2018, 12(6): 6326-6334.

[9] 王锋, 刘星辰, 王政平, 等. 基于手性超材料的太赫兹波非对称传输的研究[J]. 哈尔滨工程大学学报, 2015, 36(12): 1638-1641.
WANG F, LIU X CH, WANG ZH P, *et al*.. A study of asymmetric transmission of terahertz waves based on chiral metamaterials[J]. *Journal of Harbin Engineering University*, 2015, 36(12): 1638-1641. (in Chinese)

[10] ZHELUDEV N I, KIVSHAR Y S. From metamaterials to metadevices[J]. *Nature Materials*, 2012, 11(11): 917-924.

[11] 林婧, 李琦, 邱孟, 等. 人工原子间耦合: 超构表面调控电磁波的新自由度[J]. 中国光学, 2021, 14(4): 717-735.
LIN J, LI Q, QIU M, *et al*.. Coupling between Meta-atoms: a new degree of freedom in metasurfaces manipulating electromagnetic waves[J]. *Chinese Optics*, 2021, 14(4): 717-735. (in Chinese)

[12] 李墨馨, 王丹燕, 张诚. 超构表面结构色的原理及应用[J]. 中国光学, 2021, 14(4): 900-926.
LI M X, WANG D Y, ZHANG CH. Metasurface-based structural color: fundamentals and applications[J]. *Chinese Optics*, 2021, 14(4): 900-926. (in Chinese)

[13] 付娆, 李子乐, 郑国兴. 超构表面的振幅调控及其功能器件研究进展[J]. 中国光学, 2021, 14(4): 886-899.
FU R, LI Z L, ZHENG G X. Research development of amplitude-modulated metasurfaces and their functional devices[J]. *Chinese Optics*, 2021, 14(4): 886-899. (in Chinese)

[14] 林若雨, 吴一凡, 付博妍, 等. 超构透镜的色差调控应用[J]. 中国光学, 2021, 14(4): 764-781.
LIN R Y, WU Y F, FU B Y, *et al*.. Application of chromatic aberration control of metalens[J]. *Chinese Optics*, 2021, 14(4): 764-781. (in Chinese)

[15] GRADY N K, HEYES J E, CHOWDHURY D R, *et al*.. Terahertz metamaterials for linear polarization conversion and anomalous refraction[J]. *Science*, 2013, 340(6138): 1304-1307.

[16] CHENG Y ZH, WITHAYACHUMNANKUL W, UPADHYAY A, *et al*.. Ultrabroadband reflective polarization convertor for terahertz waves[J]. *Applied Physics Letters*, 2014, 105(18): 181111.

[17] CONG L Q, CAO W, ZHANG X Q, *et al*.. A perfect metamaterial polarization rotator[J]. *Applied Physics Letters*, 2013, 103(17): 171107.

[18] HUANG Y Y, YAO Z H, HU F R, *et al*.. Tunable circular polarization conversion and asymmetric transmission of planar chiral graphene-metamaterial in terahertz region[J]. *Carbon*, 2017, 119: 305-313.

[19] ZHANG Y, FENG Y J, ZHAO J M. Graphene-enabled tunable multifunctional metamaterial for dynamical polarization manipulation of broadband terahertz wave[J]. *Carbon*, 2020, 163: 244-252.

[20] SHEN N H, MASSAOUTI M, GOKKAVAS M, *et al*.. Optically implemented broadband blueshift switch in the terahertz regime[J]. *Physical Review Letters*, 2011, 106(3): 037403.

[21] LV T T, ZHU Z, SHI J H, *et al*.. Optically controlled background-free terahertz switching in chiral metamaterial[J]. *Optics Letters*, 2014, 39(10): 3066-3069.

[22] WANG T L, ZHANG H Y, ZHANG Y, *et al*.. Tunable bifunctional terahertz metamaterial device based on dirac semimetals and vanadium dioxide[J]. *Optics Express*, 2020, 28(12): 17434-17448.

[23] SHU F ZH, WANG J N, PENG R W, *et al*.. Electrically driven tunable broadband polarization states via active metasurfaces based on Joule-heat-induced phase transition of vanadium dioxide[J]. *Laser & Photonics Reviews*, 2021, 15(10): 2100155.

[24] ZHU W, YANG R SH, FAN Y CH, *et al*.. Controlling optical polarization conversion with $Ge_2Sb_2Te_5$-based phase-change dielectric metamaterials[J]. *Nanoscale*, 2018, 10(25): 12054-12061.

[25] 李增霖, 唐华伟, 徐文霞, 等. 太赫兹波束可调谐的编码超表面设计[J]. 电波科学学报, 2021, 36(6): 932-937.
LI Z L, TANG H W, XU W X, *et al*.. Coding metasurface design for terahertz beam shaping[J]. *Chinese Journal of Radio Science*, 2021, 36(6): 932-937. (in Chinese)

[26] ZHENG X X, XIAO ZH Y, LING X Y. A tunable hybrid metamaterial reflective polarization converter based on vanadium oxide film[J]. *Plasmonics*, 2018, 13(1): 287-291.

[27] DING F, ZHONG SH M, BOZHEVOLNYI S I. Vanadium dioxide integrated metasurfaces with switchable functionalities at terahertz frequencies[J]. *Advanced Optical Materials*, 2018, 6(9): 1701204.

[28] LUO J, SHI X ZH, LUO X Q, *et al*.. Broadband switchable terahertz half-/quarter-wave plate based on metal-$VO_2$ metamaterials[J]. *Optics Express*, 2020, 28(21): 30861-30870.

[29] 杨朝晖, 江明珠, 刘永琛, 等. 基于二氧化钒复合超表面的太赫兹带宽可调极化转换器[J]. 中国激光, 2021, 48(17): 1714001.
YANG ZH H, JIANG M ZH, LIU Y CH, *et al*.. Tunable-bandwidth terahertz polarization converter based on a vanadium dioxide hybrid metasurface[J]. *Chinese Journal of Lasers*, 2021, 48(17): 1714001. (in Chinese)

[30] LV T T, CHEN X Y, DONG G H, *et al*.. Dual-band dichroic asymmetric transmission of linearly polarized waves in terahertz chiral metamaterial[J]. *Nanophotonics*, 2020, 9(10): 3235-3242.

[31] LIU M, XU Q, CHEN X Y, *et al*.. Temperature-controlled asymmetric transmission of electromagnetic waves[J]. *Scientific Reports*, 2019, 9(1): 4097.

[32] 周高潮. 电磁偏振转换及主动调控超材料器件[D]. 南京: 南京大学, 2018: 57-58.
ZHOU G CH. Electromagnetic polarization-converting and active metamaterials[D]. Nanjing: Nanjing University, 2018: 57-58. (in Chinese)

[33] ZHANG C H, ZHOU G CH, WU J B, *et al*.. Active control of terahertz waves using vanadium-dioxide-embedded metamaterials[J]. *Physical Review Applied*, 2019, 11(5): 054016.

[34] ZHANG X Y, LI Q, LIU F F, *et al*.. Controlling angular dispersions in optical metasurfaces[J]. *Light:Science & Applications*, 2020, 9(1): 76.

Author Biographics：

LV Ting-ting (1989—), female, Tangyuan city, Heilongjiang province, lecturer, received her PhD degree from School of Physics and Optoelectronic Engineering, Harbin Engineering University in 2022. She is mainly engaged in the research of structural design and application of tunable metamaterials. E-mail: oktingting521@126.com

吕婷婷(1989—)，女，黑龙江汤原人，讲师，2022 年于哈尔滨工程大学物理与光电工程学院获得博士学位。主要从事可调谐超构材料的结构设计与应用研究。E-mail: oktingting521@126.com

SHI Jin-hui (1979—), male, Zhaodong city, Heilongjiang province, professor and doctoral supervisor, received his PhD degree in materials science from Harbin Engineering University in 2007. He is mainly engaged in the application research of metamaterials. E-mail: shijinhui@hrbeu.edu.cn

史金辉(1979—)，男，黑龙江肇东人，教授，博士生导师，2007 年于哈尔滨工程大学获得材料学博士学位。主要从事超构材料的应用研究。E-mail: shijinhui@hrbeu.edu.cn